(Received 30 October 2025, Accepted 24 November 2025, Scheduled 19 December 2025)

A 5G NR n79 Band Compact MIMO Antenna with DGS-Based Isolation Enhancement

Prabhu Kumar Kothavari and Venkata Rajasekhar Nuthakki*

School of Electronics Engineering, VIT-AP University, India

ABSTRACT: A compact four-port multiple-input multiple-output (MIMO) antenna operating on the N79 band (4.4–5.0 GHz) is designed for use in 5G wireless communication systems. The suggested antenna is synthesized over an FR4 epoxy substrate with a relative permittivity of $\varepsilon_r = 4.4$, and a standard height of 1.2 mm. The overall dimensions of the antenna are $45 \times 45 \times 1.2\,\text{mm}^3$, making it suitable for insertion into miniature 5G-enabled portable devices. A novel defected ground structure (DGS) is proposed, employing the strategic placement of two stubs of unequal lengths within the shared ground plane to effectively mitigate surface-wave propagation and thereby suppress mutual coupling among antenna elements. Thus, the design achieves considerable isolation, with a level below -20 dB across the targeted operational band. The suggested antenna operates at 4.67 GHz with a peak gain of 2.83 dBi and a radiation efficiency of 92%. The performance of the MIMO antenna was comprehensively assessed using standard diversity metrics, achieving an 0.01 envelope correlation coefficient (ECC), a diversity gain (DG) of 9.99 dB, a channel capacity loss (CCL) of 0.36 bits/s/Hz, and a mean effective gain (MEG) consistently below -3 dB. A strong correlation between experimental and simulated findings points towards the robustness of the suggested design. With its compact size, high isolation, and excellent MIMO performance, the antenna demonstrates strong potential for integration into sub-6 GHz 5G MIMO wireless communication systems.

1. INTRODUCTION

The advent of 5G networks has underscored the significance of sub-6 GHz bands, particularly n77 and n79, in high regard due to their optimal balance between coverage, penetration, and deployment cost compared to mmWave frequencies. While mmWave bands offer extremely high data rates, they suffer from severe path loss, susceptibility to blockage, and limited penetration through obstacles, making sub-6 GHz bands a more practical choice for ubiquitous deployment in both urban and rural environments [1, 2]. These mid-band frequencies also enable a smoother transition from existing 4G LTE infrastructure by supporting backward compatibility and reducing the capital expenditure for network operators. With 5G supporting massive, massive machine-type communications (mMTC), ultra-reliable low-latency communications, and enhanced mobile broadband, the design of advanced antenna architectures is essential to meet the stringent performance requirements of these diverse application scenarios [3]. MIMO and massive-MIMO techniques are fundamental to achieving high spectral efficiency and improved link reliability in sub-6 GHz deployments without requiring extra bandwidth or transmit power [4, 5]. These methods leverage spatial diversity and multiplexing benefits to improve data rates and ensure reliable signal transmission. However, increasing the number of radiating elements in a compact array intensifies the inter-element coupling and raises the envelope correlation coefficient (ECC), thereby degrading diversity efficiency and reducing the overall system efficiency [6, 7]. This makes isolation enhancement a critical design challenge in space-constrained antenna configurations. To address these issues, several decoupling techniques have been investigated, including (EBG), electromagnetic bandgap, DGS, parasitic loading, neutralization process, and element orientation diversity [8–11]. Each approach offers distinct advantages, such as suppressing surface wave propagation, introducing bandgap effects, or redirecting coupling currents to non-radiating regions. For instance, fractal-loaded MIMO antennas on $72 \times 72\,\text{mm}^2$ FR4 panels have achieved isolation levels near 28 dB, ECC below 0.005, and gain around 3.6 dBi [12]. Similarly, metasurface-based four-port MIMO systems have demonstrated isolation better than -35 dB and gain up to 9 dBi, leveraging engineered surface impedance to enhance electromagnetic performance [13]. Other works present multi-element designs using orthogonal polarization and DGS techniques, achieving ECC below 0.03 and isolation above 20 dB in compact sub-6 GHz arrays [14–16]. Despite these advances, many reported designs exhibit physically large footprints, intricate fabrication requirements, or complex feed structures, limiting their suitability for compact and low-cost wireless devices. For example, John et al. proposed a flexible dual-band MIMO antenna of size $57 \times 50\,\text{mm}^2$ with isolation exceeding 22 dB and ECC below 0.05 on an adaptable substrate, showing strong promise for wearable and conformal applications [17]. Likewise, compact two-port and eight-port designs utilizing ground stubs and radiation nulling elements have achieved competitive diversity performance in both mmWave and sub-6 GHz ranges [18, 19]. Nevertheless, there remains a clear need for designs that strike a balance between

* Corresponding author: Venkata Rajasekhar Nuthakki (rajasekhar.venkata@vitap.ac.in).

high isolation, low ECC, stable radiation characteristics, and a truly compact form factor. In response to these challenges, the proposed antenna introduces an unequal-length stub-based DGS mechanism, which progressively enhances mutual coupling suppression from approximately -12 dB to over -20 dB, a feature not reported in prior n79 MIMO designs. Additionally, the antenna achieves a compact $45 \times 45 \times 1.2\,\text{mm}^3$ footprint, which is significantly smaller than comparable 5G sub-6 GHz four-port MIMO antennas in recent literature. Comprehensive full-wave electromagnetic simulations indicate isolation better than -20 dB, an ECC lower than 0.01, and a peak gain of 2.83 dBi, all while maintaining a compact and manufacturable layout. Furthermore, a detailed parametric study investigates the influence of DGS slot dimensions, inter-element spacing, and feed positioning on the overall performance metrics. A prototype of the suggested antenna was constructed and experimentally analysed. Measured results exhibit excellent agreement with simulations, with S-parameter deviations within 0.5 dB, radiation efficiency exceeding 92%, and diversity gain above 9.99 dB. Furthermore, a comparative study with previously published sub-6 GHz MIMO antennas indicates that the suggested structure achieves competitive or better isolation, ECC, and gain, while offering a reduced footprint and avoiding complex structural modifications. The proposed solution is therefore well-suited for integration into modern 5G user equipment, small-cell base stations, and portable internet of things (IoT) devices requiring compact multi-element antennas.

The rest of this paper is structured as follows. Section 2 indicates the antenna configuration, design technique, and parametric optimization procedure. Section 3 includes both the simulated and experimental results, including a detailed comparison and performance validation. Finally, Section 4 concludes and also outlines potential scope for further improvement.

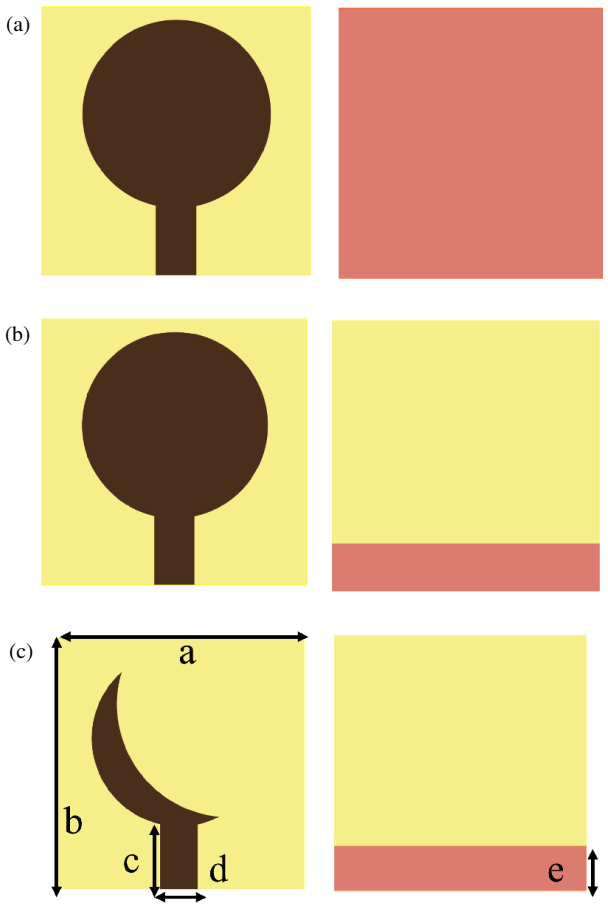

FIGURE 1. Progression of the single monopole antenna configuration top and bottom views, (a) Ant-1, (b) Ant-2, (c) Ant-3. The antenna dimensions are: $a = 20\,\text{mm}$, $b = 20\,\text{mm}$, $c = 5.1\,\text{mm}$, $d = 3\,\text{mm}$, and $e = 3.5\,\text{mm}$.

2. ANTENNA DESIGN AND METHODOLOGY

The single monopole antenna attains resonance at the specified frequency via a systematic design process by carefully modeling and optimizing several parameters. Each parameter significantly influences the antenna's resonant behavior. In particular, the ground length and the main resonator were optimized by deriving the resonator geometry through selective cutting from an initial circular structure. Fig. 1 depicts the progressive development stages of the single monopole radiator. In the initial version (Ant-1), a circular radiating element is implemented over FR4 substrate with dimensions of $20 \times 20 \times 1.2\,\text{mm}^3$, accompanied by a full ground plane. Microstrip feed line width (d) is adjusted to 3 mm aiming to achieve an impedance of $50\,\Omega$. This antenna is intended to operate in the 5G NR n79 band (4.4–5.0 GHz). However, Ant-1 fails to exhibit proper resonance due to inadequate surface current dispersion over the radiator. To enhance impedance matching and enhance radiation performance, the ground plane in Ant-2 is modified to a partial configuration. This modification significantly broadens the bandwidth of impedance, allowing the antenna to operate from 4.44 GHz to 6.31 GHz. Although Ant-2 demonstrates wideband behavior, the achieved bandwidth does not fully encompass the desired n79 band. To further shift the resonant frequency to the lower side of the band, the feedline length is extended in Ant-3. This increased length effectively elongates the electrical path for surface current flow, thereby enhancing current distribution across the radiator and lowering the fundamental resonant frequency. As a result, the modified antenna achieves full coverage of the n79 band and resonates at 4.76 GHz, exhibiting an impedance bandwidth ranging from 4.4 to 5 GHz with a fractional bandwidth of 12.7%, while maintaining good impedance matching and favorable radiation characteristics.

2.1. Four-Port Antenna Design Evolution

The single-element antenna has been expanded to a four-port MIMO design to enhance system performance by utilizing spatial diversity and mitigating multipath fading effects. The entire physical measurements of the suggested MIMO antenna are $45 \times 45 \times 1.2\,\text{mm}^3$. The antenna elements are arranged orthogonally, which increases the effective spacing between adjacent elements and thereby improves isolation. This orthogonal placement also facilitates a compact layout while maintaining the desired radiation performance. The edge-to-edge space between neighboring elements is represented as g. In MIMO systems, adding more ports increases channel capacity and di-

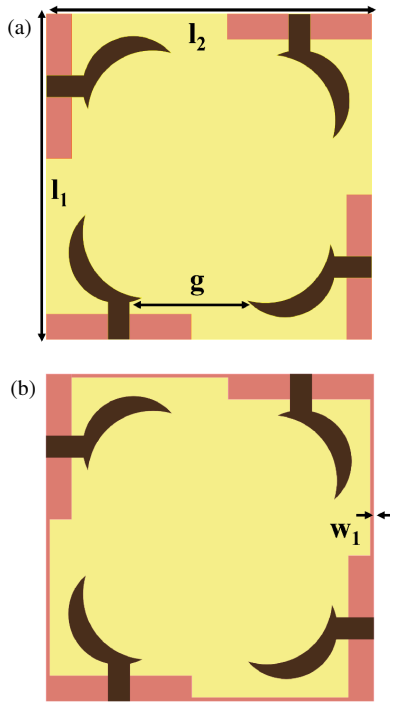

FIGURE 2. Four-port MIMO antenna configuration, (a) without common ground, (b) with common ground. The antenna dimension parameters are: $g = 14$ mm, $I_1 = 45$ mm, $I_2 = 45$ mm and $w_1 = 0.5$ mm.

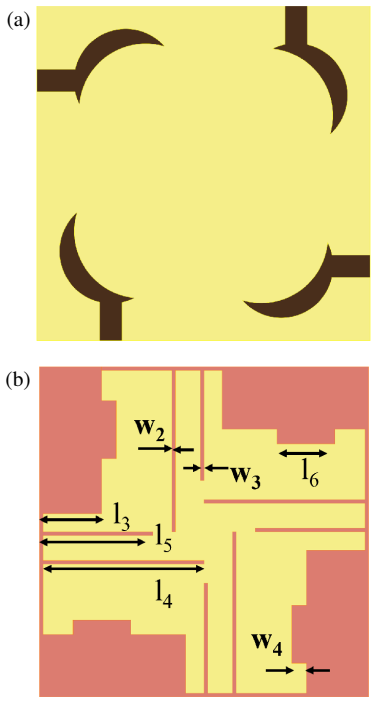

FIGURE 3. Proposed four-port MIMO antenna, (a) top view, (b) bottom view with DGS. Antenna dimensions are: $l_3 = 8.5$ mm, $l_4 = 22$ mm, $l_5 = 15$ mm, $l_6 =$ mm, $w_2 = 0.5$ mm, $w_3 = 0.5$ mm, and $w_4 = 2$ mm.

versity gain, thereby enhancing link reliability and overall data throughput. To achieve spatial diversity and mitigate mutual coupling, the radiating elements are oriented orthogonally. The theoretical minimum edge-to-edge separation required for minimal coupling is expressed as

$$g = \frac{\lambda_{\max}}{2} = \frac{c}{2f_{\min}}, \tag{1}$$

where $c = 3 \times 10^8$ m/s is the velocity of light, and $f_{\min} = 4.67$ GHz is the lowest operating frequency. Substituting these values yields $\lambda_{\max} \approx 32.115$ mm, resulting in $g \approx 64.23$ mm. However, due to the compact design constraints, the actual edge-to-edge spacing is optimized to $g = 14$ mm through parametric analysis. This corresponds to a spacing of less than a quarter-wavelength ($\lambda/4$), which is sufficient to achieve acceptable isolation and spatial diversity in a compact form factor. Fig. 2(a) depicts the layout of the suggested four-port MIMO antenna without a common ground. Enhanced inter-element spacing, denoted by g, is maintained to achieve a balance between compactness and isolation. With this optimization, the antenna attains an isolation superior -13 dB across the operational band. To quantify the mutual coupling, the coupling coefficient $|C_c|^2$ between antenna ports is given by (2).

$$|C_c|^2 = \frac{|S_{21}|^2}{\sqrt{(1-|S_{11}|^2)(1-|S_{22}|^2)}} \tag{2}$$

Assuming ideal return losses at both ports (i.e., $S_{11}, S_{22} \approx 0$), the expression is simplified to

$$|C_c|^2 \approx |S_{21}|^2 = 10^{\frac{S_{21}}{10}}. \tag{3}$$

Substituting $S_{21} = -13$ dB:

$$|C_c|^2 = 10^{\frac{-13}{10}} = 10^{-1.3} \approx 0.0501. \tag{4}$$

The isolation I between antenna ports is calculated as

$$I = -20\log_{10}(|C_c|) = -10\log_{10}(|C_c|^2). \tag{5}$$

Substituting $|C_c|^2 = 0.0501$

$$I = -10\log_{10}(0.0501) \approx -10 \times (-1.3) = 13\,\text{dB}. \tag{6}$$

This confirms the measured isolation performance. The resulting low mutual coupling and high isolation validate the effectiveness of the suggested compact sub-6 GHz MIMO antenna for practical applications. Although the use of isolated ground planes may slightly modify the surface current paths and provide marginal improvements in port-to-port isolation, this approach introduces significant electromagnetic discontinuities that degrade the structural integrity and electromagnetic compatibility of the antenna system [20]. Furthermore, isolated grounds often lead to unstable impedance matching, distorted radiation characteristics, and poor integration with RF front-end circuitry. For practical multi-port MIMO implementations, a unified ground plane is preferred, as it ensures a consistent return current path, stable impedance characteristics, and reliable radiation performance. Therefore, designs with separate ground planes are generally unsuitable for compact and ro-

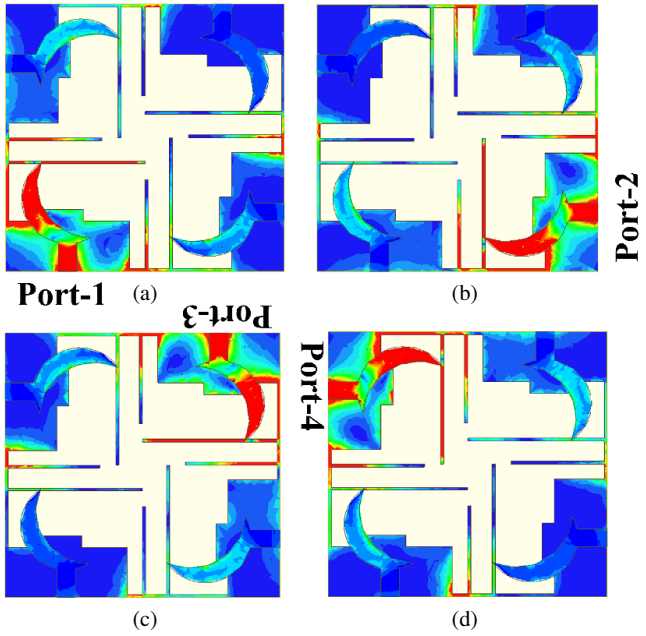

FIGURE 4. Surface current dispersion of the suggested four-port MIMO antenna at 4.67 GHz for (a) Port 1, (b) Port 2, (c) Port 3, (d) Port 4 are excited.

bust MIMO antenna systems due to their susceptibility to performance degradation and operational instability. Fig. 2(b) illustrates the four-port MIMO antenna with a common ground structure, where a strip of width w_1 is used to connect all the ground planes, forming a common ground configuration. However, with this common ground setup, the antenna fails to resonate within the targeted frequency band, and no significant isolation is observed between the ports. To further improve isolation and impedance matching, a DGS is developed. The front, rare views of the suggested antenna are indicated in Fig. 3(a) and Fig. 3(b), respectively. The height of the ground plane (l_3) is parametrized from 3.5 mm to 9.5 mm to regulate the actual electrical length of the radiator and thereby shift the operating frequency band. An optimum value of $l_3 = 8.5$ mm) enables the antenna to resonate within the target band, with a resonance observed at 4.8 GHz and mutual coupling reduced to below -12 dB due to improved impedance matching between the radiating elements. To further enhance isolation, a ground stub (l_4) is etched to suppress surface current coupling between the antenna elements. The stub length l_4 is varied between 20 mm and 23 mm, with optimum value of $l_4 = 22$ mm, and the stub width W_2 is optimized to 0.5 mm, resulting in improved current path cancellation and an isolation of approximately -15 dB. Subsequently, an additional stub l_5 is incorporated to increase the current path difference between the antenna elements, thereby reducing near-field coupling. A parametric analysis of l_5 in the range of 14–16 mm reveals that the optimal value of $l_5 = 15$ mm, along with an optimized stub width of $w_3 = 0.5$ mm, achieves an isolation level of approximately -19 dB. However, this configuration introduces a minor shift of the resonant frequency and fails to fully cover the n79 band. To overcome this limitation, a ground stub l_6 is incorporated into the ground plane. A parametric analysis is performed by varying l_6 from 7 mm to 8.2 mm, with the optimal value determined as $l_6 = 7.4$ mm. Furthermore, the width of the adjoining stub w_4 is optimized to 2 mm. These modifications enable the antenna to achieve resonance at 4.67 GHz while maintaining an isolation level below -20 dB, thereby ensuring effective operation within the 5G NR n79 band. Fig. 4 depicts the calculated surface current distribution over the suggested antenna when each port is individually activated, i.e., Ports 1 to 4, respectively. It can be observed that the active port exhibits a strong and concentrated current flow along the radiating element and the adjacent feed region, confirming efficient excitation at the intended resonant frequency. This behavior validates the effectiveness of the defected ground structure (DGS) and optimized element spacing in suppressing surface wave propagation and reducing unwanted coupling paths. The current distribution of the proposed antenna before and after introducing the DGS is illustrated in Fig. 5. The figure clearly demonstrates that the DGS effectively redirects surface currents, thereby reducing mutual coupling between adjacent elements. The step-by-step DGS evolution improves isolation by progressively disrupting the ground-plane current flow. In the first stage (I3), optimizing the ground height reduces current spreading beneath the adjacent radiators, improving isolation to approximately -12 dB. In the second stage (I4), introducing a shallow DGS notch elongates the return-current path and increases the effective inductance, raising isolation to about -15 dB. In the third stage (I5), the addition of an intermediate stub forces the surface current to split into two unequal-length branches, creating path imbalance and partial cancellation near neighboring ports, improving isolation to around -19 dB. Finally, the fourth stage (I6) incorporates a fine-tuning stub that generates a localized high-impedance region, suppressing residual leakage currents and enabling isolation better than -20 dB across the n79 band. Overall, the complete DGS evolution clearly demonstrates the effectiveness of the proposed structure in controlling surface currents and achieving strong isolation.

3. RESULTS AND DISCUSSION

The tested prototype of designed four-port antenna, showing both the front and rear views, is presented in Fig. 6(a). Antenna measurements were performed using an MS46122B vector network analyzer (VNA). The designed antenna is tested inside an anechoic chamber, as indicated in Fig. 6(b), to evaluate the radiation pattern and gain. Fig. 7 indicates the design evolution of the suggested four-port MIMO antenna. In the initial stage (Ant-1), the antenna fails to resonate within the desired frequency band. In the second stage (Ant-2), the antenna achieves resonance from 4.44 GHz to 6.31 GHz with a center frequency of 5 GHz and a minimum reflection coefficient of -27 dB. However, Ant-2 does not completely cover the N79 band. In the final stage (Ant-3), the antenna resonates from 4.39 GHz to 5.36 GHz with a center frequency of 4.76 GHz and a minimum reflection coefficient of -46 dB, providing improved impedance matching and enhanced bandwidth coverage.

Figure 8(a) illustrates the configuration of the suggested four-port MIMO antenna devoid of a common ground plane. The antenna while resonating at 4.7 GHz attained a bandwidth

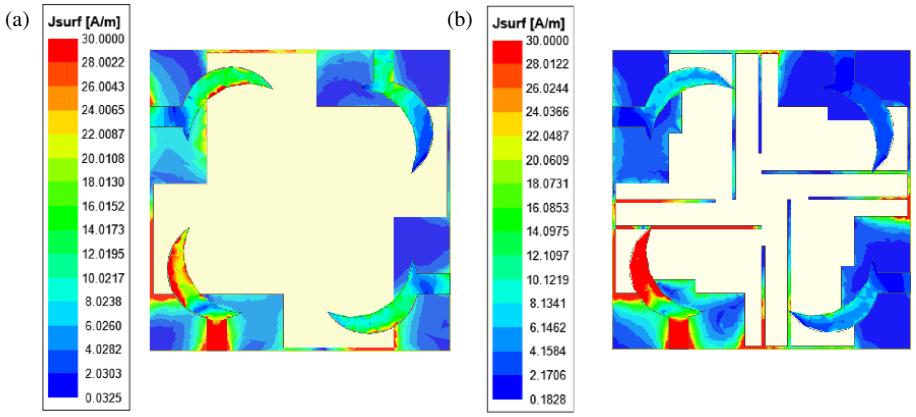

FIGURE 5. Surface current dispersion of the suggested four-port MIMO antenna at 4.67 GHz for (a) before DGS, (b) after DGS.

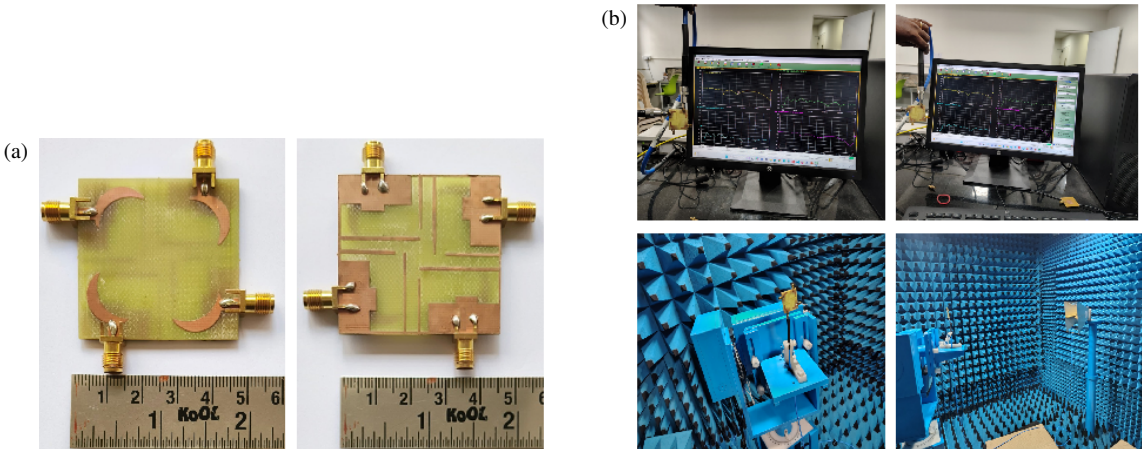

FIGURE 6. (a) Prototype showing top and bottom views. (b) Antenna testing using VNA and anechoic chamber.

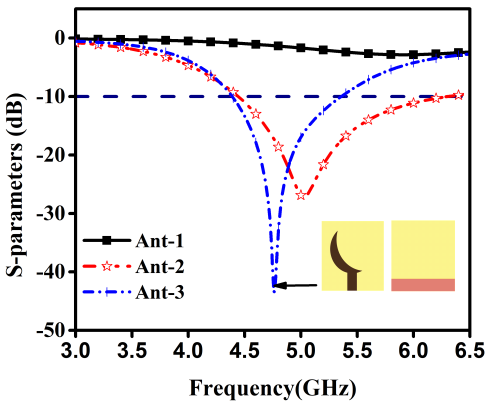

FIGURE 7. Evolution stages of the single antenna design with simulated S_{11} results.

of 4.4–5.36 GHz, with an acceptable return loss of -46 dB. The mutual coupling among antenna elements is affected by inter-element spacing g. By optimizing the spacing, the antenna achieves an isolation level of approximately -13 dB. However, practically, completely isolated grounds are challenging to implement due to fabrication constraints, which may lead to performance degradation. To address this, the four-port antenna is linked to a shared ground plane, as illustrated in Fig. 8(b). In this configuration, the antenna resonates at 3.49 GHz with a bandwidth ranging from 3.23 GHz to 3.80 GHz. However, it fails to radiate effectively within the desired frequency band, and no significant isolation is observed between the ports. These results indicate that the presence of a common ground plane considerably affecting the radiation characteristics and coupling behavior of the antenna, thereby highlighting the necessity of an optimized ground structure in the final design. Fig. 9(a) presents the parametric analysis of the ground length l_3, varied between 3.5 and 9.5 mm. At $l_3 = 8.5$ mm, the antenna operates over the 4.41–5.65 GHz band, with a resonance at 4.8 GHz and a return loss of approximately -30 dB. The corresponding isolation at this frequency is found to be -12 dB. Furthermore, Fig. 9(b) presents the S-parameters of the four-port MIMO antenna for the optimized value of l_3. Fig. 10 illustrates the parametric analysis of the l_4, and the optimal performance is observed at $l_4 = 22$ mm, where the antenna resonates between 4.18 and 4.73 GHz with a central frequency of 4.5 GHz. Fig. 10(a) presents the variation in S_{12} as l_4 changes from 20 mm to 22 mm, while the corresponding S-parameters at the optimized l_4 value are shown in Fig. 10(b). Additionally, it is confirmed that the isolation consistently remains be-

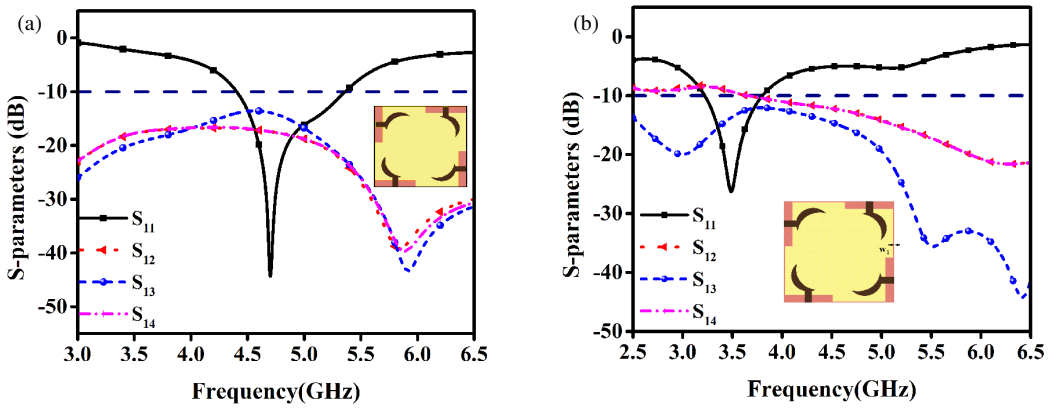

FIGURE 8. Simulated results of four-port MIMO antenna, (a) without a common ground plane, (b) with a common ground plane (without DGS).

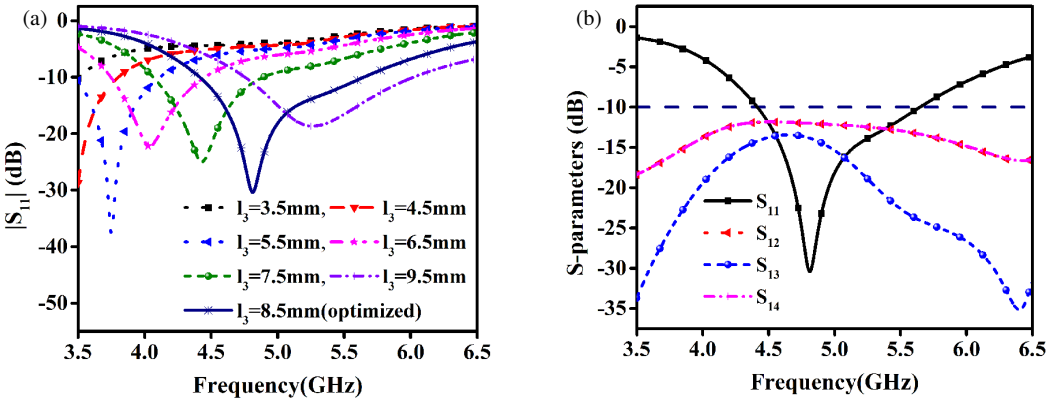

FIGURE 9. Four-port MIMO antenna with DGS: (a) parametric analysis of l_3 for S_{11}, (b) S-parameters of the four-port antenna after optimization with $l_3 = 8.5$ mm.

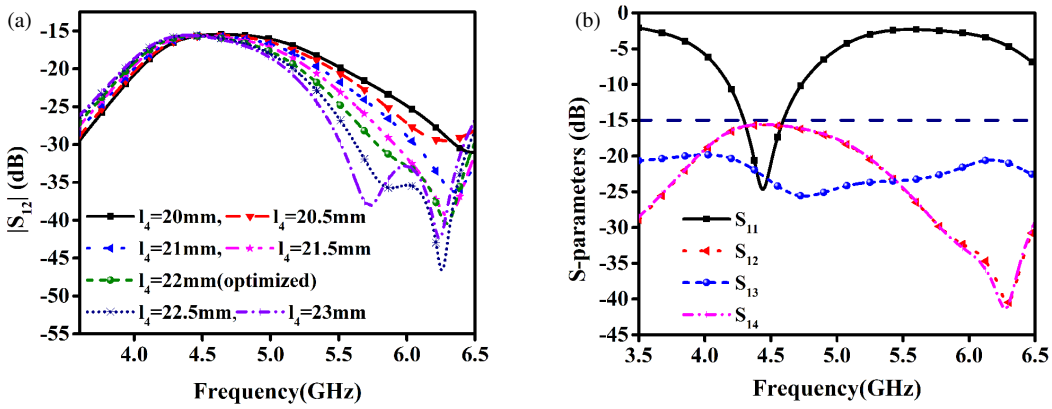

FIGURE 10. Four-port MIMO antenna with DGS. (a) Parametric analysis of l_4 for S_{12} variations. (b) S-parameters after $l_4 = 22$ mm optimization.

low -15 dB near the optimal configuration. Further enhancement in isolation is achieved through the parametric analysis of the ground stub length l_5, as presented in Fig. 11. The value of l_5 is varied between 14 and 16 mm, and the stub width W_3 is optimized to 0.5 mm. The optimized value of $l_5 = 15$ mm enables the antenna to operate within 4.30–4.83 GHz, extending the bandwidth while improving isolation to approximately -19 dB, compared to the previously achieved -15 dB. Fig. 11(a) shows the parametric analysis of the corresponding S_{12} results, while Fig. 11(b) presents the S-parameter results for different l_5 values. To further enhance bandwidth and ensure coverage of the 5G NR n79 band, an additional ground stub l_6 is incorporated into the ground plane. The optimal value is $l_6 = 7.4$ mm. The stub width is also optimized to $w_4 = 0.5$ mm. This modification shifts the resonant frequency band to 4.4–5.0 GHz, thereby achieving full n79 band coverage. Furthermore, the isolation performance has been greatly enhanced to better than -20 dB. The ultimate simulation results of the S_{11} and transmission co-

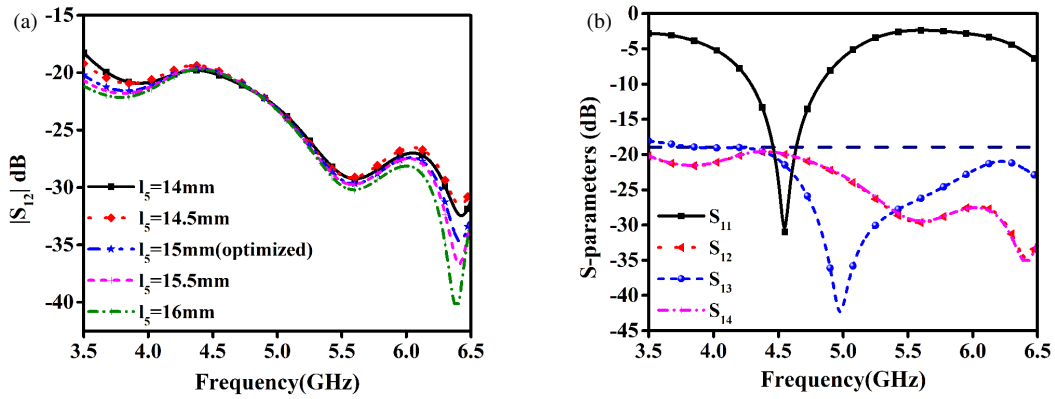

FIGURE 11. Four-port MIMO antenna with DGS: parametric analysis of stub length l_5, (a) isolation parameter S_{12} and (b) S-parameters for $l_5 = 15$ mm.

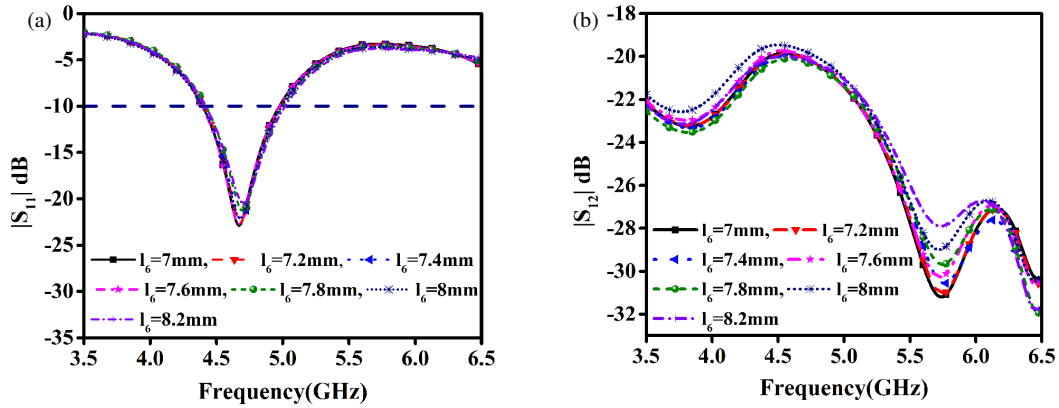

FIGURE 12. Four-port MIMO antenna with DGS: parametric analysis of l_6: (a) S_{11}, (b) S_{12} after optimization with $l_6 = 7.4$ mm.

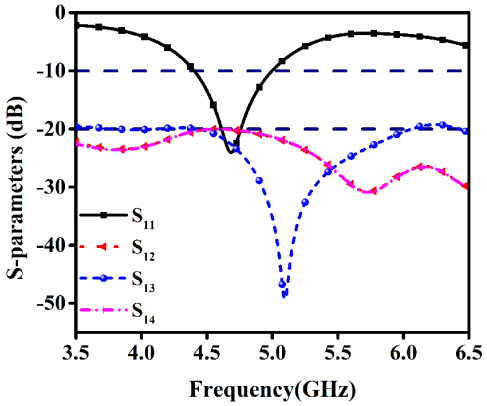

FIGURE 13. Simulated S-parameters of the proposed four-port MIMO antenna.

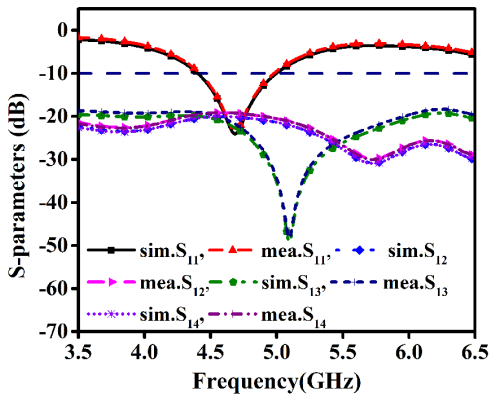

FIGURE 14. Simulated and measured S-parameters of the proposed four-port MIMO antenna.

efficient S_{12} are shown in Fig. 12(a) and Fig. 12(b), respectively. The simulated characteristics of the suggested four-port MIMO antenna are indicated in Fig. 13. The design achieves isolation levels below -20 dB and offers sufficient bandwidth to fully cover the 5G NR n79 band, confirming its suitability for sub-6 GHz MIMO applications. Fig. 14 illustrates a contrast between experimental and simulated outcomes when Port 1 is activated. A strong agreement is observed in the S_{11} responses, indicating the reliability and accuracy of antenna design proposed. Owing tothe symmetrical configuration of antenna, all four ports exhibit similar reflection and transmission characteristics. Fig. 15 illustrates the simulated and experimental diversity characteristics of the proposed MIMO antenna, encompassing ECC, DG, CCL, and MEG. ECC is a crucial statistical metric for analyzing the correlation among antenna elements, evaluating their isolation in MIMO systems. In practical scenarios, ECC is estimated based on far-field radiation patterns

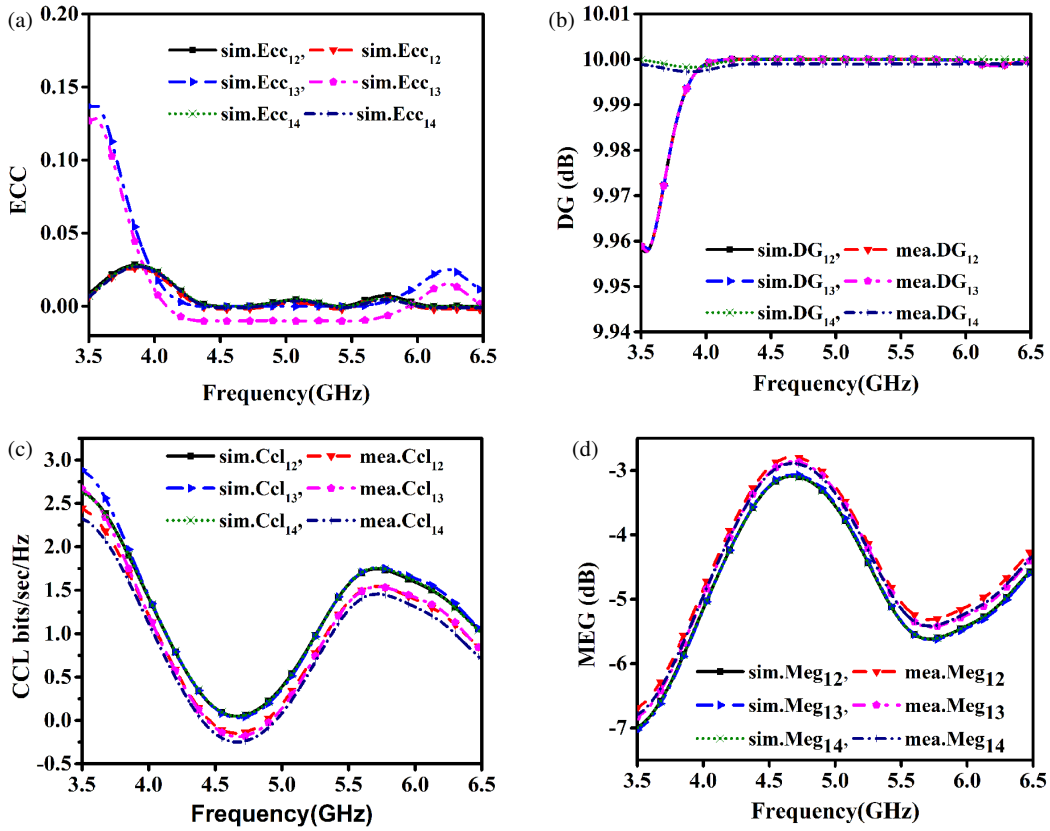

FIGURE 15. Simulated and measured diversity performance parameters of the proposed four-port MIMO antenna: (a) ECC, (b) DG, (c) CCL, and (d) MEG.

using the following expression [27].

$$\mathrm{ECC}_{ij} = \frac{\left|\int_0^{2\pi}\int_0^{\pi}\left[\vec{F}_i(\theta,\phi)\cdot\vec{F}_j^{*}(\theta,\phi)\right]\sin\theta d\theta d\phi\right|^2}{\left(\int_0^{2\pi}\int_0^{\pi}\left|\vec{F}_i(\theta,\phi)\right|^2\sin\theta d\theta d\phi\right)} \times \frac{1}{\left(\int_0^{2\pi}\int_0^{\pi}|\vec{F}_j(\theta,\phi)|^2\sin\theta d\theta d\phi\right)}. \quad (7)$$

An ECC value exceeding 0.5 is deemed acceptable for practical MIMO systems, while values under 0.01 indicate excellent isolation. The suggested antenna achieves ECC values below 0.01 in both simulated and measured outcomes, confirming superior isolation performance. Diversity Gain (DG) reflects the enhancement in signal robustness achieved through spatial diversity in MIMO systems. It is mathematically derived from the Envelope Correlation Coefficient (ECC) and is expressed as [28].

$$\mathrm{DG} = 10\sqrt{1-(\mathrm{ECC})^2} \quad (8)$$

Both simulated and experimental DG values for the proposed antenna approach are 9.99 dB, which is close to the optimal value of 10 dB, showing effective diversity efficiency. The Channel Capacity Loss (CCL) measures the reduction in system capacity caused by mutual coupling between antenna elements. It is computed using the correlation matrix $\boldsymbol{\Psi}$, as expressed below [29].

$$\mathrm{CCL} = -\log_2\left(\det(\boldsymbol{\Psi})\right) \quad (9)$$

A CCL value below 0.4 bits/s/Hz is generally desired for high-performance MIMO systems. The suggested design achieves a computed and measured CCL of approximately 0.36 bits/s/Hz, satisfying this criterion. MEG indicated the median power obtained by each antenna port in a multipath environment. It is calculated [30].

$$\mathrm{MEG}_i = \frac{1-\sum_{j=1}^{N}|S_{ij}|^2}{2}, \quad i=1,2 \quad (10)$$

For a balanced design, the MEG values for all ports should be comparable and typically fall within the range of -3 to -5 dB. The suggested antenna achieves MEG values less than -3 dB across both simulation and measurement, indicating a uniform power distribution and good diversity characteristics. The suggested four-port MIMO antenna exhibits a peak gain of 2.83 dBi at the resonant frequency of 4.67 GHz, as shown in Fig. 17. Additionally, the design achieves a 92% of radiation efficiency, which indicates minimal conductor and dielectric losses, as well as efficient impedance matching across the operating band. The values of stable gain and efficiency across the desired frequency range further confirm the robustness of the proposed structure for real-world wireless communication environments. Fig. 16 attains the experimental and computed radiation patterns of the suggested antenna operating at different

TABLE 1. Performance comparison of MIMO designs.

Reference (Year)	Size (mm^3)	Frequency (GHz)	Isolation (dB)	ECC/DG	Gain (dBi)	Efficiency (%)
PA (This Work)	$45 \times 45 \times 1.2$	4.4–5.0	−20	0.01/9.99	2.83	92
[21]	$158 \times 60 \times 1.6$	4.8–5.0, 5.925–6.4	−17	0.10/NR	2.5	82
[22]	$50 \times 50 \times 1.6$	4.38–5.19	−13.9	0.066/NR	2.8	68.6
[23]	$90 \times 90 \times 1.57$	3.56–5.28	−15	0.01/NR	2.8	88
[24]	$60 \times 60 \times 1.6$	4.5–5.0	−16	0.02/9.98	2.6	85
[25]	$65 \times 65 \times 1.6$	4.3–5.0	−16	0.025/9.97	2.9	84
[26]	$55 \times 55 \times 1.6$	4.4–5.1	−14	0.04/9.94	2.7	80

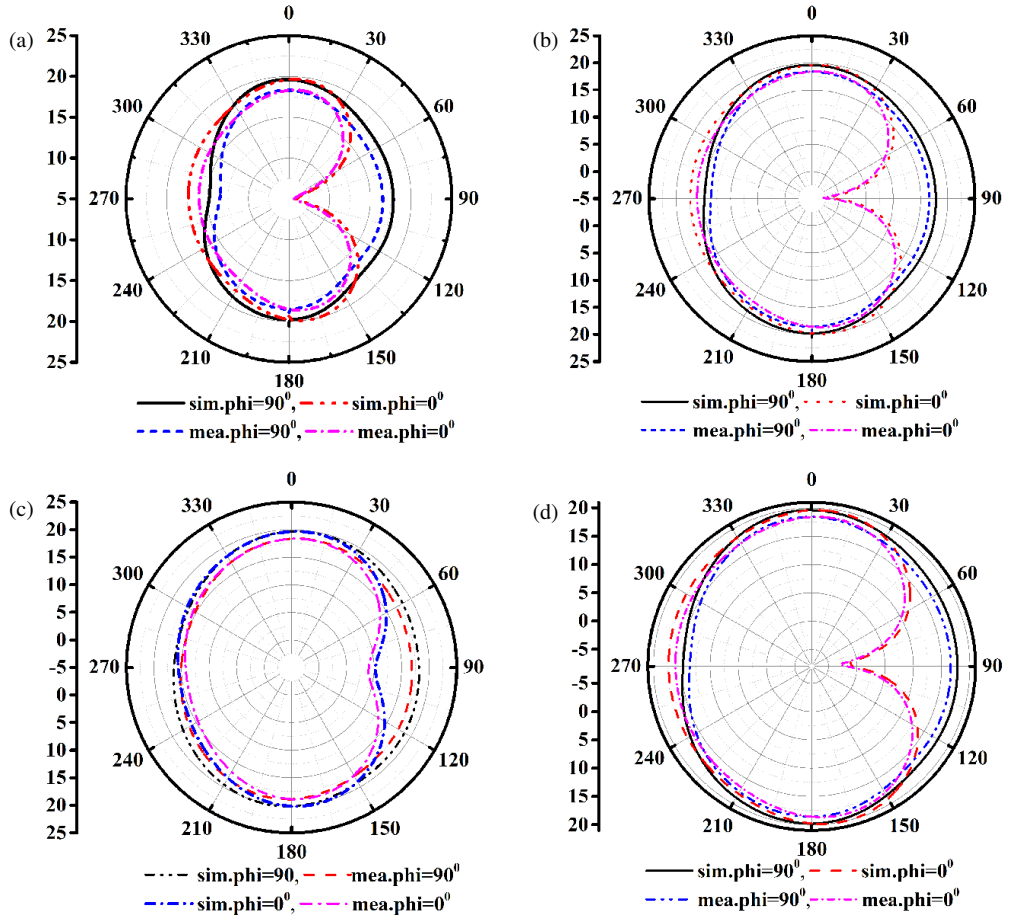

FIGURE 16. Simulated and measured radiation patterns of the proposed MIMO antenna at (a) 4.4 GHz, (b) 4.67 GHz, (c) 4.8 GHz and (d) 5 GHz.

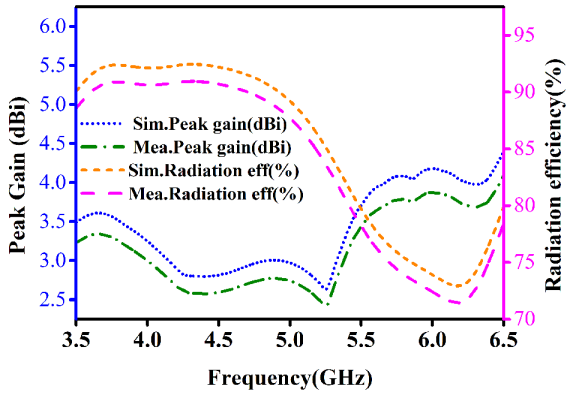

FIGURE 17. Simulated and measured peak gains and radiation efficiencies of the proposed four-port MIMO antenna.

frequencies, 4.4 GHz, 4.67 GHz, 4.85 GHz, and 5.0 GHz. The E-plane patterns maintain a stable and nearly omnidirectional distribution across the operating band, which is advantageous for consistent signal reception in various device orientations. Similarly, the H-plane exhibits a broadside radiation characteristic with minimal deformation over the frequency range, supporting uniform spatial power distribution in MIMO configurations. This stability across multiple frequencies indicates that the defected ground structure (DGS) and optimized element geometry effectively enhance isolation without degrading far-field performance. Such consistent radiation behavior ensures reliable coverage for sub-6 GHz wireless communication systems, even under varying operational scenarios.

Table 1 provides a detailed comparison between the suggested four-port MIMO antenna and recently reported designs

in terms of overall size, operating frequency band, isolation performance, gain, efficiency, and all MIMO diversity parameters. The findings indicate that the proposed design achieves a compact footprint while maintaining superior isolation and radiation characteristics, proving its high suitability for 5G sub-6 GHz MIMO applications.

4. CONCLUSION

This work has presented and evaluated a compact four-port MIMO antenna tailored for N79 band operation (4.4–5.0 GHz). The design is realized on a cost-effective FR4 substrate with a geometry of $45 \times 45 \times 1.6\,\text{mm}^3$, ensuring suitability for integration into modern portable 5G devices. The inclusion of a novel defected ground structure (DGS) and the strategic placement of two stubs with unequal lengths within the common ground effectively suppress surface-wave propagation and minimize mutual coupling, resulting in isolation levels consistently above 20 dB without compromising impedance matching. The antenna is centered at 4.67 GHz, offering a peak gain of 2.83 dBi with a radiation efficiency of 92%. The multiple-input multiple-output (MIMO) performance was examined using standard diversity metrics, achieving an ECC of 0.01, a DG of approximately 9.99 dB, a CCL of around 0.36 bits/s/Hz, and MEG maintained below -3 dB. Strong correlation between the simulation and measurement outcomes reinforces the reliability and practical viability of the proposed structure. With its reduced form factor, high isolation capability, and favorable diversity characteristics, the proposed antenna represents a promising solution for sub-6 GHz 5G MIMO wireless communication systems.

ACKNOWLEDGEMENT

The authors would like to sincerely thank VIT University, Vellore, for providing access to the essential facilities and technical environment required for antenna testing. The support provided by the institution greatly contributed to the experimental validation and overall success of this research.

REFERENCES

[1] Wei, X., J. Lu, Y. Miao, J. Huang, Z. Chen, and G. Liu, "High isolation MIMO antenna system for 5G N77/N78/N79 bands," *Micromachines*, Vol. 15, No. 6, 721, 2024.

[2] Elabd, R. H., A. J. A. Al-Gburi, and A. A. Megahed, "Compact circular MIMO antenna with defected ground structure (DGS) for improved isolation in 5G sub-6 GHz mobile systems," *Results in Engineering*, Vol. 27, 105737, 2025.

[3] Sharma, P., R. N. Tiwari, P. Singh, P. Kumar, and B. K. Kanaujia, "MIMO antennas: Design approaches, techniques and applications," *Sensors*, Vol. 22, No. 20, 7813, 2022.

[4] Li, M., L. Jiang, and K. L. Yeung, "A general and systematic method to design neutralization lines for isolation enhancement in MIMO antenna arrays," *IEEE Transactions on Vehicular Technology*, Vol. 69, No. 6, 6242–6253, 2020.

[5] Addepalli, T., M. S. Kumar, C. R. Jetti, N. K. Gollamudi, B. K. Kumar, and J. Kulkarni, "Fractal loaded, novel, and compact two- and eight-element high diversity MIMO antenna for 5G sub-6 GHz (N77/N78 and N79) and WLAN applications, verified with TCM analysis," *Electronics*, Vol. 12, No. 4, 952, 2023.

[6] Ahmed, B. T. and I. F. Rodríguez, "Compact high isolation UWB MIMO antennas," *Wireless Networks*, Vol. 28, 1977–1999, 2022.

[7] Xi, S., J. Cai, L. Shen, Q. Li, and G. Liu, "Dual-band MIMO antenna with enhanced isolation for 5G NR application," *Micromachines*, Vol. 14, No. 1, 95, 2023.

[8] Hasan, M. M., M. T. Islam, T. Alam, P. Kirawanich, S. Alamri, and A. S. Alshammari, "Metamaterial loaded miniaturized extendable MIMO antenna with enhanced bandwidth, gain and isolation for 5G sub-6 GHz wireless communication systems," *Ain Shams Engineering Journal*, Vol. 15, No. 12, 103058, 2024.

[9] Ali, H., X.-C. Ren, I. Bari, M. A. Bashir, A. M. Hashmi, M. A. Khan, S. I. Majid, N. Jan, W. U. K. Tareen, and M. R. Anjum, "Four-port MIMO antenna system for 5G n79 band RF devices," *Electronics*, Vol. 11, No. 1, 35, 2022.

[10] Babu, K. V., S. Das, S. S. Ali, M. El Ghzaoui, B. T. P. Madhav, and S. K. Patel, "Broadband sub-6 GHz flower-shaped MIMO antenna with high isolation using theory of characteristic mode analysis (TCMA) for 5G NR bands and WLAN applications," *International Journal of Communication Systems*, Vol. 36, No. 6, e5442, 2023.

[11] El Ouahabi, M., A. Dkiouak, D. El Hadri, A. Zakriti, and M. Charif, "A low-profile four-port MIMO antenna for 5G-n79 band with high diversity performance," *Advanced Electromagnetics*, Vol. 13, No. 1, 44–49, 2024.

[12] Chen, Y.-T. and H.-L. Su, "A sub-6 GHz 8×8 MIMO antenna array for 5G metal-frame mobile phone applications," *Electronics*, Vol. 13, No. 23, 4590, 2024.

[13] Salehi, M. and H. Oraizi, "Wideband high gain metasurface-based 4T4R MIMO antenna with highly isolated ports for sub-6 GHz 5G applications," *Scientific Reports*, Vol. 14, No. 1, 14448, 2024.

[14] John, D. M., T. Ali, S. Vincent, S. Pathan, J. Anguera, B. Virdee, R. M. David, K. Nayak, and S. P. Gopi, "A dual-band flexible MIMO array antenna for sub-6 GHz 5G communications," *Sensors*, Vol. 25, No. 11, 3557, 2025.

[15] Rizvi, S. N. R., M. A. Sufian, W. A. Awan, Y. Choi, N. Hussain, and N. Kim, "A closely spaced two-port MIMO antenna with a radiation null for out-of-band suppressions for 5G sub-6 GHz applications," *PLoS One*, Vol. 19, No. 7, e0306446, 2024.

[16] Sharma, N., P. Jha, M. Saxena, and D. Saxena, "DGS based eight-port MIMO antenna for 5G(N-79) and sub-6 GHz applications," in *2024 IEEE 11th Uttar Pradesh Section International Conference on Electrical, Electronics and Computer Engineering (UPCON)*, 1–4, Lucknow, India, 2024.

[17] Narayana, M. V., G. Immadi, A. Navya, M. V. Swathi, M. Nikhitha, B. Vineetha, and G. C. A. S. Swaroop, "Analysis of a quad port dual band MIMO antenna for sub-6 GHz applications," *Progress In Electromagnetics Research B*, Vol. 105, 137–151, 2024.

[18] Addepalli, T., "Compact MIMO diversity antenna for 5G sub: 6 GHz (N77/N78 and N79) and WLAN (Wi-Fi 5 and Wi-Fi 6) band applications," *Wireless Personal Communications*, Vol. 132, No. 3, 2203–2223, 2023.

[19] Tang, G., T. Xiao, L. Cao, R. Cheng, C. Liu, L. Huang, and X. Xu, "A multi-frequency low-coupling MIMO antenna based on metasurface," *Electronics*, Vol. 13, No. 11, 2146, 2024.

[20] Zhang, S. and G. F. Pedersen, "Mutual coupling reduction for UWB MIMO antennas with a wideband neutralization line," *IEEE Antennas and Wireless Propagation Letters*, Vol. 15, 166–169, 2015.

[21] Zahid, M., Q. Ali, N. Bhowmike, D. P. Bolla, S. Shoaib, and Y. Amin, "Dual-band MIMO antenna for n79 and sub-7 GHz

smartphone applications," *Electronics*, Vol. 13, No. 14, 2724, 2024.

[22] Natali, Y., D. W. Astuti, C. Apriono, *et al.*, "Study on defected ground structure models with miniaturized patches for broadband wireless systems," *Journal of Communications*, Vol. 19, No. 3, 168–174, 2024.

[23] Upadhyaya, T., V. Sorathiya, S. Al-Shathri, W. El-Shafai, U. Patel, K. V. Pandya, and A. Armghan, "Quad-port MIMO antenna with high isolation characteristics for sub 6-GHz 5G NR communication," *Scientific Reports*, Vol. 13, No. 1, 19088, 2023.

[24] Abdelghany, M. A., A. A. Ibrahim, H. A. Mohamed, and E. Tammam, "Compact sub-6 GHz four-element flexible antenna for 5G applications," *Electronics*, Vol. 13, No. 3, 537, 2024.

[25] Das, G. S., B. B. Chamuah, Y. Beria, P. P. Kalita, and A. Buragohain, "Compact four elements sub-6 GHz MIMO antenna for 5G applications," *Materials Today: Proceedings*, 2023.

[26] Yousef, B. M., A. M. Ameen, A. Desai, H.-T. Hsu, V. Dhasarathan, and A. A. Ibrahim, "Defected ground structure-based wideband circularly polarized 4-port MIMO antenna for future Wi-Fi 6E applications," *AEU — International Journal of Electronics and Communications*, Vol. 170, 154815, 2023.

[27] Senger, S. and P. K. Malik, "A comprehensive survey of massive-MIMO based on 5G antennas," *International Journal of RF and Microwave Computer-Aided Engineering*, Vol. 32, No. 12, e23496, 2022.

[28] Ahmed, H., A. M. Ameen, A. Magdy, A. Nasser, and M. Abo-Zahhad, "A dual-port wideband MIMO antenna for sub-6 GHz 5G applications," *Suez Canal Engineering, Energy and Environmental Science*, Vol. 3, No. 3, 31–41, 2025.

[29] Alanazi, M. D. and S. K. Khamas, "A compact dual band MIMO dielectric resonator antenna with improved performance for mm-Wave applications," *Sensors*, Vol. 22, No. 13, 5056, 2022.

[30] Moses, A. T. Z. and N. Moses, "Compact self decoupled MIMO antenna pairs covering 3.4–3.6 GHz band for 5G handheld device applications," *AEU — International Journal of Electronics and Communications*, Vol. 141, 153971, 2021.